IOSR Journal of Electrical and Electronics Engineering (IOSR-JEEE)
e-ISSN: 2278-1676,p-ISSN: 2320-3331, Volume 11, Issue 6 Ver. I (Nov. – Dec. 2016), PP 95-115
www.iosrjournals.org

Mechatronic Modeling and Control of a Nonlinear Variable-Speed Variable-Pitch Wind Turbine by Using the Bond Graph Approach

Zakaria Khaouch[1], Mustapha Zekraoui[1], Nourreeddine Kouider[1], Mustapha Mabrouki[1] , Jamaa Bengourram
[,1]*Industrial Engineering Laboratory, Faculty of Science and Technology, Sultan MoulaySlimane University, BeniMellal, Morocco.*

Abstract:*As wind turbines increased in size and power, control specifications became more challenging and regulation mechanisms more sophisticated. More and more reliable and powerful model control strategies are needed not only to keep the turbine within its safe operating region but also to improve efficiency and quality of power conversion. This paper mainly focuses on the mechatronic modeling and control of a 5MW Variable-Speed Variable-Pitch Wind Turbine (VS-VP WT) for the above-rated power operating condition. The principal parts of the wind turbine are modeled by using the Bond-Graph approach and the control strategy is realized by combining a torque control with a blade pitch control strategy by means of bicausality of the bond graph. The robustness of the proposed model control is verified and the simulation of the complete model is conducted for variable wind speed operation conditions.*

Keywords:*Mechatronic modeling, control, Bond graph, Wind turbine, Variable-Speed, Variable-Pitch Pitching system, Torque control, Bicausality, Inverse model.*

I. Introduction

Since ancient times, the wind has been exploited in different ways, mainly for grain milling and water pumping. A wind turbine is essentially a device that capture part of the wind energy and converts it into useful work. Wind turbines can be classified into four categories [1], namely: Fixed-Speed Fixed-Pitch (FSFP), Fixed-Speed Variable-Pitch (FSVP), Variable-Speed Fixed-Pitch (VSFP) and Variable-Speed Variable-Pitch (VSVP). Compared to Variable-Speed (VS), Fixed-Speed (FS) are easy to construct and operate, but VS have the advantages of improved energy capture, reduction in transient load and better power conditioning[2]. Advanced control plays an important role in the performance of large wind turbines. This allows better use of resources of the turbine, increasing the lifetime of mechanical and electrical components, and earning higher returns. The controllers presented in this paper are designed for VSVP wind turbines operating at high wind speeds. The primary objectives of the controllers can be arranged in the following topics: Maximization of energy capture taking account of safe operation restrictions such as rated power, rated speed and cut-out wind speed on the one hand, and preventing the WECS from excessive dynamic mechanical loads on the other hand. This general goal encompasses transient loads alleviation, high frequency loads mitigation and resonance avoidance, finally keeping the rotor power at design limits when the wind speed is above its rated value. Two control inputs are available: the generator torque and the blade pitch angle. Wind turbine controllers objectives depend on the operation area[3, 4]. VSVP wind turbine operation can be divided into four operating regions (Fig. 1):

- Region I: Below cut-in wind speed.
- Region II: Between cut-in wind speed and rated wind speed.
- Region III: Between rated wind speed and cut-out wind speed.
- Region IV: Upper than cut-out wind speed.

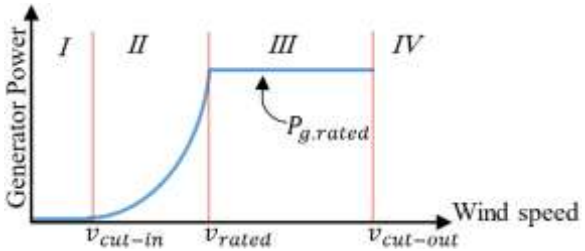

Fig. 1 Operating regions of the wind turbine

In region I, wind turbines do not run because power available in the wind is low compared to losses in the turbine system. Region II is an operational mode where it is desirable that the turbine capture as much power as

possible from the wind, this is due to the fact that wind energy extraction rates are low and the structural loads are relatively small. The generator torque provides the control input to vary the rotor speed, while the blade pitch is held constant. Region III is encountered when the wind speeds are high enough; then the turbine must limit the fraction of the captured wind power such that safe electrical and mechanical loads are not exceeded. If wind speeds exceed contains the region III (region IV), the system will make a forced stop of the machine, protecting it from excessively high aerodynamic loads. In practice, the passage from region II to region III is somewhat unusual. In fact, the electromagnetic torque in region II controls the rotor speed, and in region III it is the power that should be controlled by the blade pitch control.

Many works have proposed controllers to work around an operating point using control of the generator torque to keep the turbine at a condition of maximum power point tracking, e.g., [5]. Some previously published works proposed pitch control methods to limit the rotor speed at high wind speeds, e.g., [6]. In [7] a combination of proportional integral (PI) and SMC is used to adjust the turbine rotor speed for extracting maximum power without estimating the wind speed. In [8] a PI based torque control is used to control the WT, where optimal gains are achieved by particle swarm optimization and fuzzy logic theory, [9]discussed the multivariable control strategy by combining the nonlinear state feedback control for region II with linear control for region III. Finally, the results are compared with the existing control strategies such as PID and LQG. WT control using adaptive radial basic NN used for both pitch and torque controllers is addressed in [10]. Active disturbance rejection based pitch control for variable speed WT is presented in [11]. Relatively few works suggest control strategies based on varying operating conditions for wind turbines and their dynamics and using a unified approach in modeling and control of the wind turbine. The principal aim of this paper is to show same benefits of the bond graph in modeling and control of the wind turbine. In this subject, a wind turbine mechatronic model is developed. The main components of the system are modeled using the Bond-Graph Approach (BGA). The control law is derived by combining a torque control strategy with a pitch control by using the inverse model of the bond graph; a compression with a PID controller is done to validate the propos model control. The implementation of the complete model and its control system has been carried out by means of the 20-Sim simulation program.

The paper is organized as follows. Section 2 discusses the modeling of the WT by using the BGA. Problem formulation and control objectives are discussed in Section 3. The proposed controllers for all the regions are discussed in Section 4. Section 5 discusses the validation of the results using the 20-Sim simulator. Finally in Section 6 a conclusion is drawn from the obtained results, which show that the proposed bond graph model control is working fine for controlling the WT at below and above rated wind speeds.

II. System modeling of the wind turbine by using the Bond graph Approach (BGA)

The wind turbine studied in this paper is a 5 MW horizontal axis and is a variable speed variable pitch wind turbine. The specifications of this turbine are described in [12] and some of its parameters are shown in Appendix A. Based on it, the mechatronic model of the wind energy conversion systems (WECS) can be stated, and the main components of a WECS will be presented by using the bond graph approach (BGA). Our primary objective is to show some of the benefits of the BGA in contributing to a model of wind turbine and presenting a nonlinear model of a wind turbine in a unified framework, containing aerodynamic system, drive train, tower, generator and pitching system.

A mechatronics model, of the entire WECS, can be structured as several interconnected subsystem models as shown in Fig. 2.

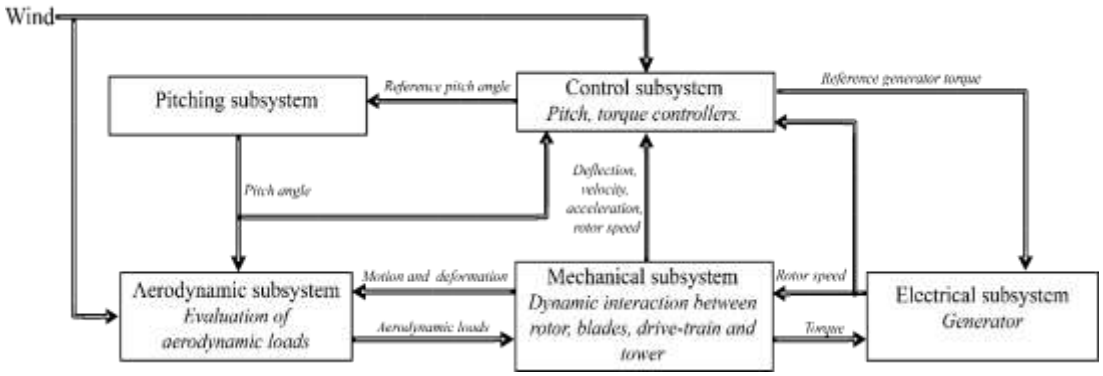

Fig. 2 Subsystem-level block diagram of a WECS

The aerodynamic subsystem describes the transformation of the wind speed field into forces on the blades that generate the rotational motion. The mechanical subsystem can be divided into two functional blocks, i.e., the drive-train and the support structure. The drive-train transfers the aerodynamic torque on the blades to the generator shaft. It encompasses the rotor, the transmission and the mechanical parts of the generator. The structure

is made up of the tower. The electrical subsystem describes the conversion of mechanical power at the generator shaft into electricity. Finally, the actuator subsystem models the pitch servo behavior. In order to analyze the system in the same reference frame, the BGA [13, 14] is used.

The bond graph is a graphical way of modeling the analysis and control of multidisciplinary systems (independent of the physical nature of the studied system), precisely due to its graphical nature of displaying the power exchange in a system, which includes storage, dissipation and transformation. Paynter, the inventor of bond graphs [15], published his first book in 1959. Karnopp et al. later extended the approach in [16], where the presentation starts with the basic elements and leads to sophisticated mathematical models suitable for automated computer simulation.

2.1 Aerodynamics bond graph model

The wind turbine rotor transforms the absorbed kinetic energy of the air into mechanical power. The power in the wind is proportional to the cube of the wind speed and can be described as[17]:

$$P_{wind} = \frac{1}{2}\rho\pi R^2 v^3 \qquad (1)$$

Whereρ is air density, R is rotor radius of the wind turbine blade, and v is wind speed. A wind turbine can only extract part of the power from the wind. The ratio of the power $C_p(\beta,\lambda)$ extracted from the wind is a nonlinear function of the blade pitch angle β and the tip-Speed Ratio λ. Therefore, the mechanical power of the wind turbine extracted from the wind can be expressed as [17]:

$$P_{mech} = \frac{1}{2}\rho\pi R^2 v^3 C_p(\beta,\lambda) \qquad (2)$$

With:

$$\lambda = \frac{R\omega_r}{v} \qquad (3)$$

Whereω_r is the speed of the turbine rotor. From (2) we can find the aerodynamic torque and the thrust force acting on the tower:

$$T_a = \frac{1}{2}\rho\pi R^2 v^3 C_q(\beta,\lambda) \qquad (4)$$

$$F_T = \frac{1}{2}\rho\pi R^2 v^2 C_T(\beta,\lambda) \qquad (5)$$

Where$C_q(\beta,\lambda)$ is the torque coefficient given as: $Cq(\beta,\lambda) = \frac{C_p(\beta,\lambda)}{\lambda}$ and $C_T(\beta,\lambda)$ is the thrust force coefficient. A generic equations is used to model $C_p(\beta,\lambda)$ and $C_T(\beta,\lambda)$. These equations are based on the modeling turbine characteristics of [18]. The power coefficient used in the calculation of the torque is given in (6). A plot of the $C_p(\beta,\lambda)$ curve is shown in Fig. 3; the plot is made with different pitch angle and tip-speed ratio. Similar formulas can be found regarding the thrust force coefficient $C_T(\beta,\lambda)$; in our calculations only a simple relation is used:

$$C_p(\beta,\lambda) = c_1\left(\frac{c_2}{\lambda_i} - c_3\beta - c_4\right)e^{-\frac{c_5}{\lambda_i}} + c_6\lambda \qquad (6)$$

$$\lambda_i = \frac{1}{\frac{1}{\lambda + 0.08\beta} - \frac{0.035}{\beta^2 + 1}} \qquad (7)$$

Where :c_1=0.5179, c_2=116, c_3=0.4, c_4=5, c_5=21 and c_6=0.0068.

In the aerodynamics part, we need to find a way to convert the wind into torque and thrust force, i.e. to transform a flow into efforts. This is done by means of a modulated gyrator MGY. We use the torque and thrust force equations given in (4) and (5). In this case the transformation is dependent on three varying parameters: the wind speed v, the pitch angle β, and the rotor rotational speed ω_r. Fig. 4 shows the bond graph model of the aerodynamics part.

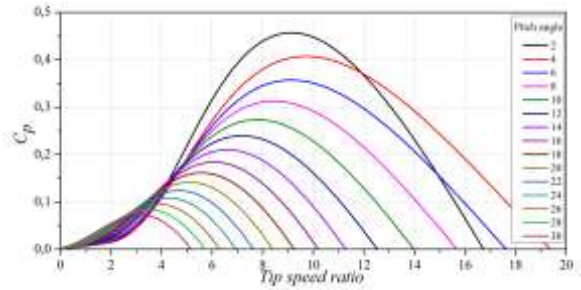

Fig. 3 Curve of Cp

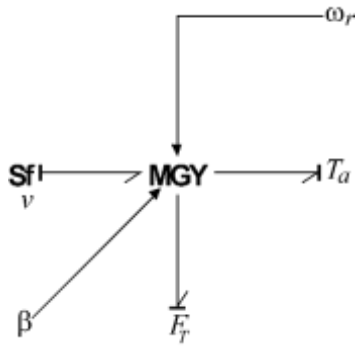

Fig. 4 Bond graph model of the aerodynamics part

2.2 Mechanical subsystem model

The mechanical subsystem includes all mechanical components of the wind turbine system; it can be divided in two flexible structures, the drive train and the tower. In this system, the rotor of the turbine, the transmission elements (gearbox) and the rotor generator composes the drive train. This can be modeled as a multi-body system (MBS) with multiple degrees of freedom. Fig. 5 shows, a sketch of a two-mass drive train model, a more detailed bond graph model is presented in [19]. The bond graph representation of the drive train is shown in Fig. 6. The model consists of two 1-junctions and two 0-junctions. The rightmost 1-junction connected to the rotor inertia J_r and rotor external damping D_r describes the rotor rotational speed ω_r. Since there are dynamics in between the rotor inertia and the generator inertia, they do not have the same speed. This is the reason for the 0-junction in the main and high speed. The 1-junction connected to the R-element (D_{ms}, D_{hs}) and the C-element (k_{ms}, K_{hs}) describe respectively the damping and stiffness in the main and high-speed shafts; the gearbox is modeled by a simple TF-element where (N_g) is the gearbox ratio, the generator inertia (J_g) and external damping (D_g) are respectively modeled by the I-element and the R-element.

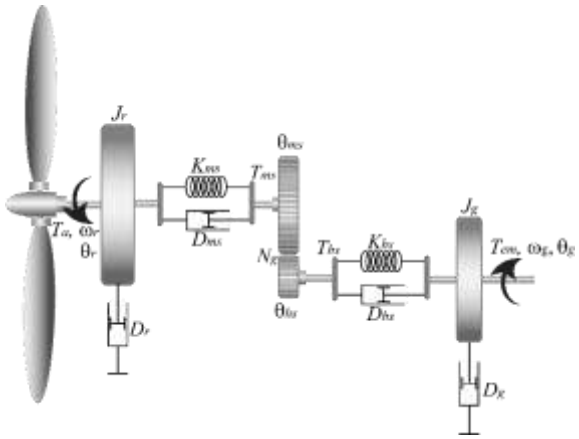

Fig. 5 Sketch of a two-mass drive train

For the tower model it is assumed that the tower moves only in horizontal direction (Fig. 7) and does not influence the mechanical system; it only affects its input, i.e. the wind speed. The bond graph model of the tower is sketched in Fig. 8, where m_t is the tower mass, F_t is the thrust force acting on the tower,D_t is the tower damping and K_t is the tower stiffness.

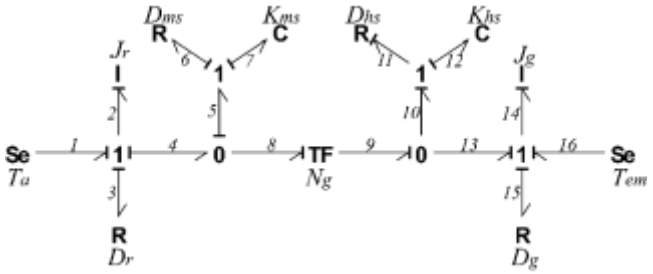

Fig. 6 Bond graph model of a two-mass drive train

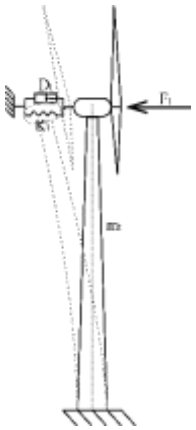

Fig. 7 Sketch of wind turbine structure

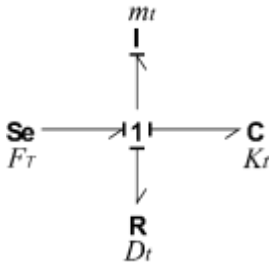

Fig. 8 Bond graph model of tower motion

2.3 Generator model

The induction generators are largely the most popular electric machines in WECS industry to convert mechanical power to electric power. In our system, a simple first-order generator model is used for the wind turbine and, accordingly, the generator torque T_{em} can be described as:

$$\dot{T}_{em} = \frac{1}{\tau}(T_{em} - T_{ref}) \quad (8)$$

2.4 Pitching Subsystem

In WECS, one of the operational problems is the variability and discontinuity of wind. In most cases, wind speed can fluctuate rapidly. Hence, the quality of produced energy becomes an important problem. Several control techniques have been designed to improve the quality of power generated from wind turbines. Pitch control is the most efficient and popular power control method, especially for variable-speed wind turbines. It is a useful method for power regulation above the rated wind speed by changing the pitch angle of the rotor blades. The actuator that drives the blades around their longitudinal axes was extensively modified to make it suitable for controls testing. The original hydraulically actuated pitch system was replaced by a high-speed electromechanical pitch system. The electromechanical system consists of a servo drive electronics box that drives a permanent magnet servo motor. This motor is connected to a gearbox that in turn drives the blade through a pinion and a bull gear system (Fig. 9). There are many possibilities to model the electric motor with different levels of complexity and accuracy. The detailed method depends on the motor type. In our model, we use a DC motor for controlling the pitch angle. Fig. 9 shows also the equivalent circuit of motor in which the armature coil is represented by resistor *R* and inductor *L* in series.

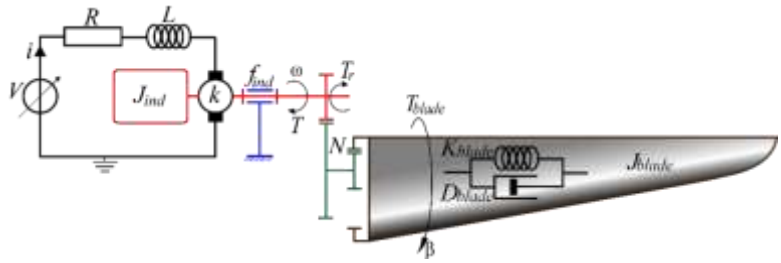

Fig. 9 Sketch of the pitching system

The torque generated by a DC motor can be explained as:

$$T = K_T I \quad (9)$$

Where$I$ is the current through conductor and K_T is the torque constant. The back emfV_b is directly proportional to angular velocity ω of rotation. Thus the back emf is given as:

$$V_b = K_v \omega \quad (10)$$

WhereK_v is constant back emf.

If we assume there are no losses in the magnetic field, then, for conservative transformation $K_T = K_v = K$ which satisfies $T\omega = V_b I$. Therefore, we can draw the bond graph model of the pitching system as shown in Fig. 10, where the coil resistance -featuring the rotor losses, is represented by an R-element R and the motor inductance by an I-element L. The electromechanical transformation is modeled as a gyrator K. The mechanical part includes all mechanical components of the pitching system: the rotor of the electric motor is represented by I-element J_{ind}, the bearing damping of the rotor is represented by R-element f_{ind}, and the transmission elements (gearbox) are represented by TF-element N. The dynamic behaviors presented in the blades are represented by R-element D_{blade} and C-element K_{blade}. The rotor blade inertia is represented by I-element J_{blade}.

Fig. 10 Bond graph of the pitching system

From the Fig. 10, we can observe an causality problem in the rightmost 1-jonction, this problem can be reserved by coming down the I-element (J_{ind}) and R-element (f_{ind}) next to the elements J_{blade} and D_{blade}. The simplified bond graph is shown in Fig. 11.

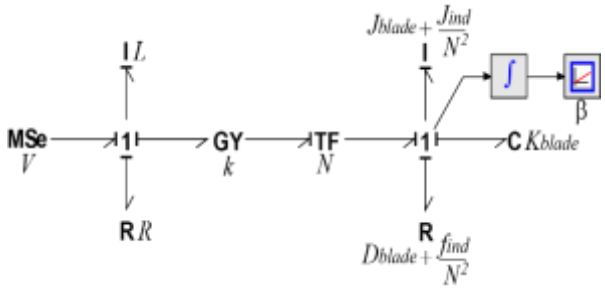

Fig. 11. Simplified bond graph model of pitching system

2.5 Complete System

The individual subsystems presented in previous sections are combined in a global system as shown in Fig 12. The inputs of the aerodynamic subsystem are connected by the wind sources, the hub speed and the pitch angle, the latter representing the primitive of the rotation speed at the pitching subsystem's output. The output torque of the aerodynamic subsystem symbolizes the mechanical subsystem's input applied on the turbine rotor. Mechanical subsystem's output is the mechanical power, which represents the electrical subsystem's input. Pitching subsystem's output is the pitch angle, and its input is the control law.

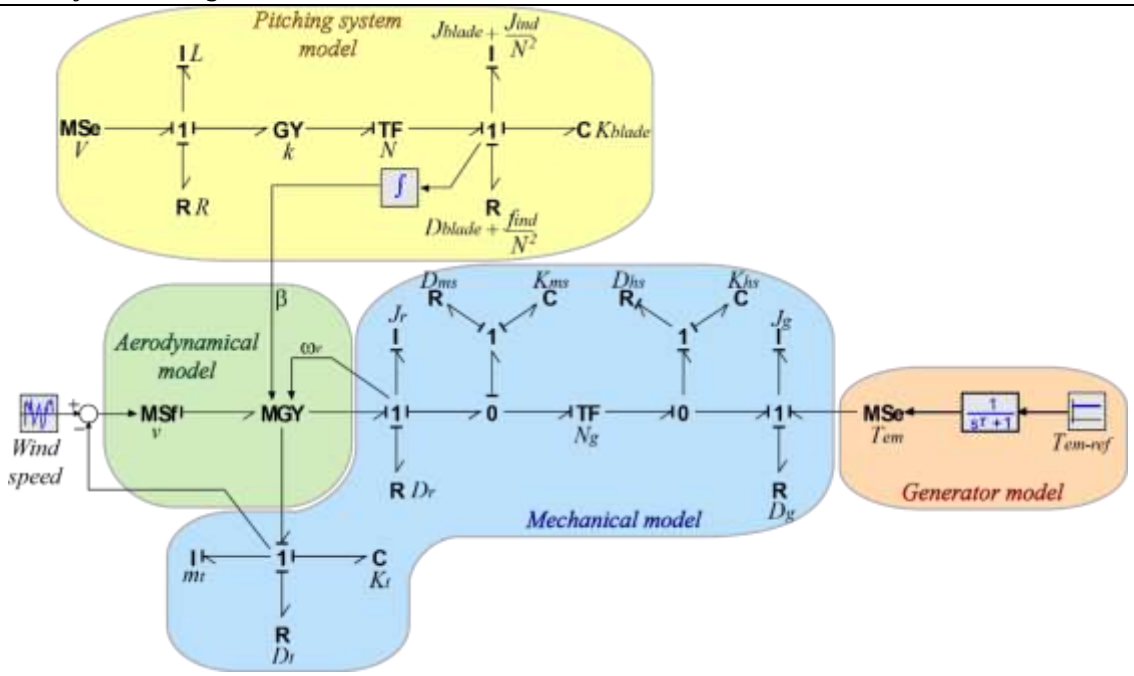

Fig. 12 Complete System

III. Selection of the Operating Point

Selection of the operating point is critical to preserving aerodynamic stability in the wind turbine system. The rotational speed ωref operating point and the blade-pitch β_{ref} operating point were selected for each wind speed using the following algorithms.

A wind turbine normally works in different operating modes along the wind speed range. It can be divided into four regions shown in Fig. 1. The wind speeds; considered as the limits of this division, include cut-in wind speed $v_{cut\text{-}in}$, rated wind speed v_{rated} and cut-out wind speed $v_{cut\text{-}out}$[20]. The values of the 5MW wind turbine studied in this paper are presented in appendix A. The control objectives in these regions are substantially different.

Being below cut-in wind speed $v_{cut\text{-}in}$ (region I), the wind turbine power generation is very low and hence not economical. Thus, the control unit shown in Fig. 2 issues the stop command and the brakes will stop the wind turbine. In this region, the pitch angle is usually set at 90°[20].

In region II, which is called the partial-load region, the wind speed is higher than $v_{cut\text{-}in}$but lower than v_{rated}; the objective is to capture as much energy as possible. In this case, the power coefficient C_p should be set to maximum power coefficient C_{pmax}. This occurs when both the tip-speed ratio λ and the pitch angle β are maintained as close as possible to their optimum values λ_{op} and β_{op}, since $C_{pmax} = C_p(\lambda_{op},\beta_{op})$. In Fig. 3, the maximum C_p value over the entire surface occurs at a pitch angle of 2° and a tip-speed ratio of 9; the rotational speed operating point ω_{op} for each wind speed in this region is:

$$\omega_{op} = \frac{\lambda_{op}}{R} v \qquad (11)$$

When the generator speed does not exceed the rated generator speed, the reference speed is:

$$\omega_{ref} = \omega_{op} \qquad (12)$$

Moreover, when the generator speed exceeds the rated generator speed, the reference speed is:

$$\omega_{ref} = \omega_{rated} \qquad (13)$$

Therefore, the rotational speed is varied in proportion to the wind speed by properly controlling the generator torque. Fig. 13 shows the structure of this generator torque control method in wind turbines using the inverse bond graph method.

In region III, which is called the full-load region, the wind speed is higher than vrated but lower than the $v_{cut\text{-}out}$. The main control purpose in this region is to keep the generator power P_g around the nominal generator power P_n, by keeping the generator speed ω_g around its rated value $\omega_{g\text{-}rated}$. This is achieved through tuning the

pitch angle of the blades. Accordingly, the control unit must send the suitable pitch angle reference β_{ref} to set the pitch angle of the blades [20].

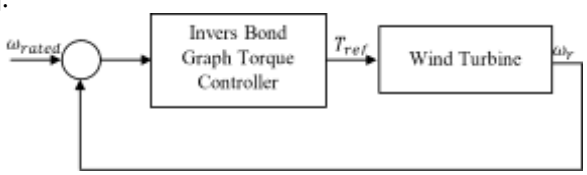

Fig. 13 Structure of the proposed torque controller

In this region, the optimum tip-speed λ_{op} and the maximum power coefficient C_{pmax} are respectively:

$$\lambda_{op} = \frac{R\omega_{rated}}{v} \qquad (14)$$

$$C_{p\max}(\beta_{op}, \lambda_{op}) = \frac{P_n}{\frac{1}{2}\rho\pi R^2 v^3} \qquad (15)$$

Where P_n is the rated turbine power. By using Fig. 3, we can calculate the value of β_{op}, since:

$$\beta_{ref} = \beta_{op} \qquad (16)$$

Fig. 14 shows the structure of the pitch controller in wind turbines using the inverse bond graph method.

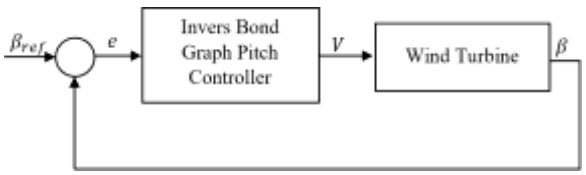

Fig. 14 Structure of the proposed pitch controller

The optimal values of λ, C_p, pitch angle β and the reference speed ω_{ref} for each wind speed (Fig. 15) for regions II and III can be calculated by using the algorithm presented here.

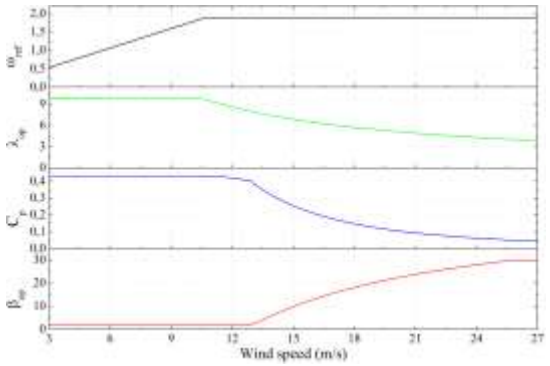

Fig. 15 Reference parameters

In region IV, where the wind speed is very high (higher than vcut-out), in order to protect the wind turbine from fatigue damages and mechanical stresses, the wind turbine must be shut down. Thus, like the procedure in region I, the control unit issues the stop command and the brakes will stop the wind turbine. In this case, the pitch angle is usually set at 90°.

The focus of this paper is on full-load region and partial-load region (regions II and III) to design an optimal generator torque and pitch controllers.

IV. Torque Control Model

In order to control the rotational speed of the electric machine and obtain the best efficiency and quality power at a wide range of operation, many electric machines equipped with power converters have been proved in industrial applications [21]. For this study, the electric machine is modeled by a first order transfer function, therefore, the electromagnetic torque developed at any instant is:

$$T_{em} = \frac{1}{\tau s + 1} T_{me-ref} \qquad (17)$$

WhereT_{em} is the electromagnetic torque, T_{ref} is the reference torque, and τ is the time constant.
The maximum power extraction techniques allow determining the speed of the turbine that achieves maximum power generated. For the 1-junction placed between bonds 13, 14, 15 and 16 of the bond graph presented in Fig. 6, we can write:

$$e_{13} + e_{16} = e_{14} + e_{15} \quad (18)$$

Where: $e_{13} = T_{mg}$: which is the mechanical torque from the gearbox, $e_{16} = -T_{em}$, $e_{14} = J_g(d\omega_g/dt)$, where J_g is the inertia of the generator and ω_g is the generator angular velocity and $e_{15} = D_g\omega_g$, where D_g is the generator external damping.

Since we can write:

$$J_g \frac{d\omega_g}{dt} = T_{mg} - D_g\omega_g + T_{em} \quad (19)$$

It can be seen that the mechanical speed is influenced by the action of two torques: the mechanical torque from the gearbox and the electromagnetic torque from the electric machine. The torque control structure presented in this paper adjusts the electromagnetic torque to set the wind turbine speed at its rated speed. In order to control the electromagnetic torque, it is necessary to generate the reference electromagnetic torque. To this aim, a specific algorithm is designed, based on the bicausal bond graph [22] and the performance of the system is compared with a conventional PID controller to validate it.

The inverse model corresponds to a re-organization of the equations where the input and output roles are exchanged: inputs become outputs and vice versa [23]. The inverse model is created by imposing both effort and flow information from the sensor and receiving both at the source. This procedure, where both informations can be imposed on a bond, cannot be done through normal causality. This is why, the notion of bicausality[24, 25] is introduced. Bicausality notation splits the causality assignment for the two factors of power, namely effort and flow. By separating the causal strokes, it allows imposing two complementary informations at one end of a bond.

In the inverse model, the source element (Se or Sf) is replaced by a source sensor (SeSf) element [23, 24] and the sensor element (De or Df) is replaced by a sensor source (DeDf) element. The difference between the source sensor and the sensor source lies in the causality of the element: the source sensor element receives information of both power variables, whereas the signal source element supplies both. The rule for bicausal 0 (1)-junction is that only one bond can bring effort (flow) information and other bonds can bring the flow (effort) information. This means that at a bicausal junction, there must be one bond bringing in both effort and flow information while there must be another bond taking out both effort and flow information. Thus, at every junction, only two bonds must be bicausal (not more, not less).

To arrive at the inverse model, bicausality is propagated from the original sensor to the original source. In the process, some internal bonds in the model are assigned bicausality such that it is propagated to the receiving source sensor.

The structure of the control in an open loop is designed with the inverse bond graph. The decoupling actions are defined (inverse matrix and disturbance compensation). The open loop structure is then extended to a closed loop control by fixing the dynamics of errors.

In our model, the input variable is the electromagnetic torque Tem and the output variable is the rotor speed ω_r of the turbine. The analysis of the direct bond graph model of Fig. 6 indicates that there is a power line and a causal path between the input variable T_{em} and the output variable ω_r. Therefore, the model is structurally invertible compared to the pair of variables T_{em} and ω_r. The objective of the controller established here is to calculate the electromechanical torque required to set the turbine rotor speed to a reference. For this calculation, it is appropriate to inverse the bond graph model of Fig. 6 relatively to the pair of variables T_{em} and ω_r.

The inverse bond graph model of the system is given in Fig. 16; the sensor (Df) and source (Sf) have been replaced with source sensor (SeSf) element and sensor source (DeDf) element. Note that fixed sources (those which are not control inputs) are retained as they are, e.g., Se: Ta at bond number 1. The SeSf element in bond number 0 imposes both effort and flow information, thereby forcing differential causality in the I-element at bond number 2. Likewise, three more storage elements are forced to assume differential causality. The DeDf element at bond number 16 receives both flow and effort information.

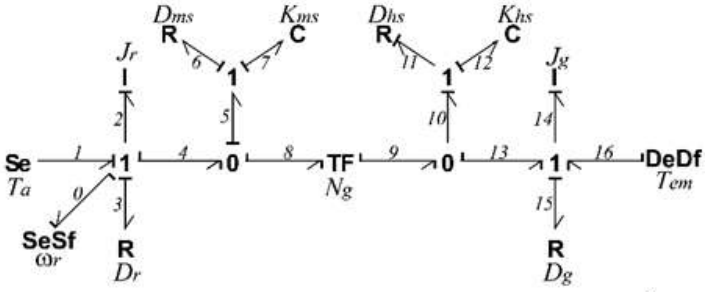

Fig. 16 Inverse bond graph for calculation of the controls laws.

From Fig.16, we can write the following from the constitutive relations of the leftmost 1-junction (i.e. 1-junction placed between bonds 0, 1, 2, 3 and 4):

$$\begin{cases} f_0 = f_1 = f_2 = f_3 = f_4 \\ e_4 = e_1 - e_0 - e_2 - e_3 \end{cases} \quad (20)$$

where: $f_0 = \omega_r$, $e_0 = 0$, $e_1 = T_a$, $e_2 = J_r(d\omega_r/dt)$ and $e_3 = D_r\omega_r$. Therefore:

$$\begin{cases} f_4 = \omega_r \\ e_4 = T_a - J_r \dfrac{d\omega_r}{dt} - D_r\omega_r \end{cases} \quad (21)$$

To establish the closed loop control law, the dynamics of the error are set in (22) as:

$$\dot{\varepsilon} + k_1\varepsilon = 0 \quad (22)$$

Where k_1 represents the controller to be used and $\varepsilon = \omega_{ref} - \omega_r$, is the error. Expression (21) becomes (23) as:

$$\begin{cases} f_4 = \omega_r \\ e_4 = T_a - J_r(\dot{\omega}_{ref} - \dot{\varepsilon}) - D_r\omega_r \end{cases} \quad (23)$$

Finally,

$$\begin{cases} f_4 = \omega_r \\ e_4 = T_a - J_r\dot{\omega}_{ref} - J_r k_1(\omega_{ref} - \omega_r) - D_r\omega_r \end{cases} \quad (24)$$

For the neighboring 0-junction in Fig. 15, we can write:

$$\begin{cases} f_8 = f_4 - f_5 \\ e_4 = e_5 = e_8 \end{cases} \quad (25)$$

From the 1-jonction between bonds 5, 6 and 7 we have:

$$\begin{cases} f_5 = f_6 = f_7 \\ e_5 = e_6 + e_7 \end{cases} \quad (26)$$

with:

$$\begin{cases} e_6 = D_{ms} f_6 = D_{ms} f_5 \\ e_7 = K_{ms}\int f_7 dt = K_{ms}\int f_5 dt \end{cases} \quad (27)$$

Therefore:

$$f_5 = \frac{1}{K_{ms}}(\dot{e}_5 - D_{ms}\dot{f}_5) \quad (28)$$

Proceeding in the same way, from the TF-element we can write:

$$\begin{cases} f_9 = N_g f_8 \\ e_9 = \dfrac{e_8}{N_g} \end{cases} \quad (29)$$

From the 0-junction placed between bonds 9, 10 and 13, we have:

$$\begin{cases} f_{13} = f_9 - f_{10} \\ e_9 = e_{10} = e_{13} \end{cases} \quad (30)$$

where:

$$f_{10} = \frac{1}{K_{ms}}(\dot{e}_{10} - D_{ms}\dot{f}_{10}) \quad (31)$$

For the rightmost 1-junction, we can write:

$$\begin{cases} f_{16} = f_{13} \\ e_{16} = -e_{13} + e_{14} + e_{15} \end{cases} \quad (32)$$

where:
$e_{16} = -T_{em}$, $e_{14}=J_g(d\omega_g/dt)$, $e_{15}=D_g\omega_g$.
Finally:

$$\begin{cases} f_{16} = f_{13} \\ -T_{em} = -e_9 + J_g\dot{\omega}_g + D_g\omega_g \end{cases} \quad (33)$$

To generate the reference electromechanical torque the generator model must be inversed as:

$$T_{em-ref} = \tau\dot{T}_{em} + T_{em} \quad (34)$$

The controller block diagram derived from these equations is shown in Fig. 17. It is important to notice that the structure of the control law contains a feed-forward control with a derivative action. Fig. 17 shows that the proposed gain is a PI controller; the estimate values are considered in the control law.

In the block diagram model, the desired output is the input. The output of the block diagram model is the reference electromagnetic torque. The block diagram contains four derivative (*d./dt*) blocks. It was simulated for the numerical parameters given in Appendix A.

V. Pitch Controller

For the above rated wind speed the generator power is fixed to its rated value that is, maximum value of the control input. In this condition, a linear pitch control is introduced. The blade pitch angle is adjusted to maintain the generated power constant in its rated value. The form of the blades and, more generally, the turbine characteristics play a key role in this power control.

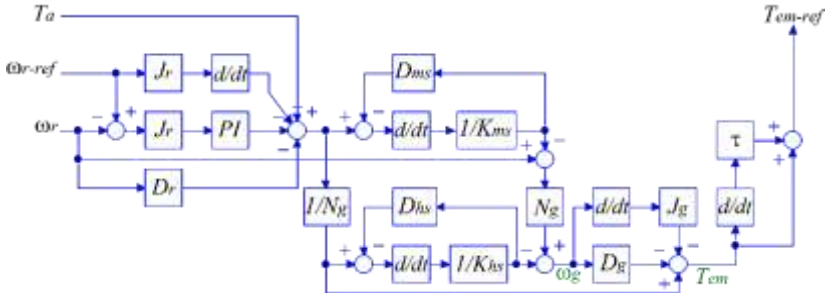

Fig. 17 Torque control law block diagram

The non-linear model of the turbine makes complex to design an analytical model of this controller. Moreover, very large differences (due to elasticity) may appear a turbine to another. That is why it is more practical to use an experimental characteristic of the blade pitch angle measured for a different wind speed. The inverse control characteristic can give directly for different wind speed the corresponding blade pitch angle; this is achieved by using the algorithm given in section 3 and the controller should provide suitable motors voltage in its output. This is obtained by using the inverse bond graph model of the pitching system.

The analysis of the bond graph model of Fig. 11 indicates that there is a power line and a causal path between the input variable V and the output variable β. Therefore, the model is structurally invertible.

The inverse bond graph model of the pitching system is given in Fig. 18, as previously mentioned, the sensor (Df) and source (Sf) have been replaced with source sensor (SeSf) elements. The SeSf element in bond number 10 imposes both effort and flow information; the DeDf element at bond number 1 receives both flow and effort information.

As previously defined in the torque controller, we can derive the equations from the inverse bond graph of the Fig. 18.

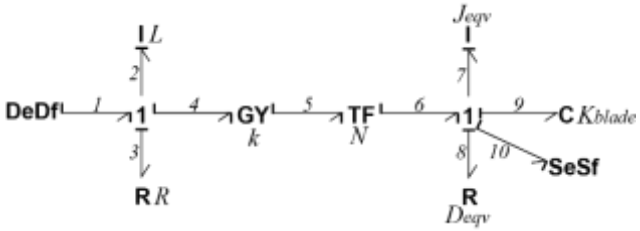

Fig. 18 Inverse bond graph for calculation of the control law of the pitch system

From Fig. 18, we can write the following from the constitutive relations of the rightmost 1-junction (i.e. 1-junction placed between bonds 6, 7, 8, 9, and 10):

$$\begin{cases} f_6 = f_7 = f_8 = f_9 = f_{10} \\ e_6 = e_7 + e_8 + e_9 + e_{10} \end{cases} \quad (35)$$

where$f_{10} = d\beta/dt$, $e_{10} = 0$, $e_9 = K_{blade}\beta$, $e_8 = D_{eqv}(d\beta/dt)$ and $e_7 = J_{eqv}(d^2\beta/dt^2)$. Therefore:

$$\begin{cases} f_6 = \dot{\beta} \\ e_6 = J_{eqv}\ddot{\beta} + D_{eqv}\dot{\beta} + K_{blade}\beta \end{cases} \quad (36)$$

To establish the closed loop control law of the pitch angle the dynamics of the error are set as (the controlled variable is a generalized displacement):

$$\begin{cases} \varepsilon = \beta_{ref} - \beta \\ \ddot{\varepsilon} + k_2\dot{\varepsilon} + k_3\varepsilon = 0 \end{cases} \quad (37)$$

Wherek_2 and k_3 represent the controllers to be used. Expression (36) becomes (48) as:

$$\begin{cases} f_6 = \dot{\beta} \\ e_6 = J_{eqv}(\ddot{\beta}_{ref} + k_2(\dot{\beta}_{ref} - \dot{\beta}) + k_3(\beta_{ref} - \beta)) \\ + D_{eqv}\dot{\beta} + K_{blade}\beta \end{cases} \quad (38)$$

From the TF-element and GY-element we can write:

$$\begin{cases} f_5 = \dfrac{f_6}{N} \\ e_5 = Ne_6 \end{cases} \quad (38)$$

$$\begin{cases} f_4 = \dfrac{e_5}{k} \\ e_4 = ke_5 \end{cases} \quad (39)$$

Finally, for the leftmost 1-junction, we can write:

$$\begin{cases} f_1 = f_2 = f_3 = f_4 = i(t) \\ e_1 = V(t) = e_2 + e_3 + e_4 = L\dfrac{di(t)}{dt} + Ri(t) + e_4 \end{cases} \quad (40)$$

We can derive a block diagram model from the bicausalled bond graph model to control the pitch angle, which is shown in Fig. 19. The proposed gains (k_2 and k_3) are PI controllers; the estimate values are considered in the control law.

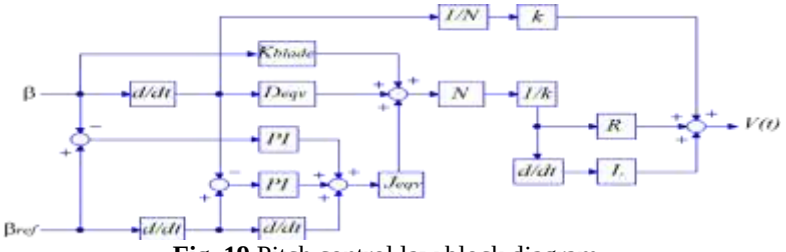

Fig. 19 Pitch control law block diagram

The bond graph representation of the complete system is shown in Fig. 20. The inputs to the systems are pitch angle, reference parameters and wind speed. It can be seen that the wind turbine control system basically contains two control loops, one is the pitch control loop and the other is the torque control loop. These two control loops operate simultaneously, but only one of them is dominant depending on the operation region shown in Fig. 1. When the wind speed is below rated speed, the torque control loop is used to regulate the turbine speed to capture maximal wind power. When the wind speed exceeds rated speed, the pitch control loop is used to provide adequate pitch angle to regulate power at its rated value.

VI. Simulation and Discussion

In order to verify the effectiveness and the robustness of the proposed control law, a simulation is carried out by using different turbulent winds to drive the wind turbine, and a comparison between the proposed controller and the conventional PI controller is done by considering these wind profiles. The PI parameters are generated using Ziegler and Nichols methods [26].

Firstly, we consider the wind profile as shown in Fig. 21, secondly, we use a turbulent wind with mean speed *12.5m/s* and finally, the performance of the control system is tested during a turbulent wind with mean speed *18m/s*.

The wind speed profile as shown in Fig. 21 changes in step of every *20sec* starting from *6m/s* to *16m/s*. This shows that both the above and below rated wind speeds are included in the wind profile. For below rated wind speed, the torque control comes into action with constant pitch angle, and for above rated wind speed, the pitch control comes into action with rated power.

Fig. 22 shows the generator speed for the proposed method (inverse bond graph (IBG)) and PID controller for below and above rated wind speeds. Both controllers achieve the nominal value of the generator speed at *80sec*. The corresponding wind speed is around *11m/s* which can be seen from Fig. 21. As the wind speed approaches the rated speed, the WT generator speed reaches the nominal value, that is, *112.35rad/s.*Figs. 23 and 24 show respectively the electrical power and the power coefficient comparison for IBG and PID controllers for the transition period. In region 2 IBG is able to extract more power than PID. Fig. 25 shows the generator torque comparison in region 2 for IBM and PID. It can be observed that IBM produces more generated torque compared to PID in region II. As the generator speed remains constant from 80sec onwards it is obvious that IBM captures more power compared to PID. Fig. 26 shows the pitch angle comparison for PID and IBG; pitch variation is found to be more for PID compared to IBG. Therefore, the pitch actuator needs more control action for PID. Fig. 27 shows the tower displacement comparison for PID and IBG. It can be observed that tower displacement in IBG is less than PID controller.

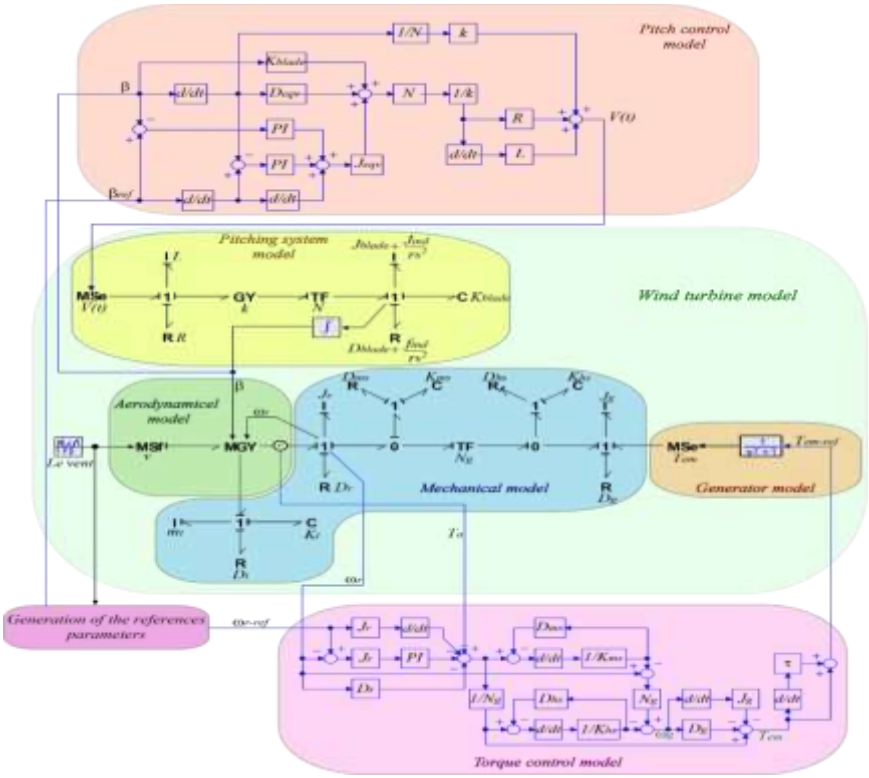

Fig. 20 Bond graph model and its control system of the wind turbine

In order to create the appropriate conditions of comparing the two methods, the wind speed profile shown in Fig. 28 with *12m/s* average wind speed is used.

As is shown in Fig. 29, the turbine rotor speed remains around its rated value *112.35rad/s*. Fig. 30 shows the generator torque; in order to increase generator power, generator torque, generator speed or both must be increased. Figs. 29 and 30 show that the generator speeds and torque in the proposed method are higher in comparison with the conventional PID. Wind turbine power, shown in Fig. 31, reaches its rated value of *5MW*. Figs. 31 and 32 demonstrate that the proposed method is able to capture more electrical power in comparison with the other controller. From Fig. 33, we find that the pitch system can track turbulent wind around cut-in speed. Therefore, according to the simulation results, the proposed method has a more effective performance in the generator torque control and pitch control in comparison with the conventional PID method; the tower displacement in IBG is less than PID controller as shown in Fig. 34.

The control system performance is also tested during a turbulent wind with mean speed *18m/s*, as shown in Fig. 35. Turbine rotor speed, generator torque, power, power coefficient, pitch angle and tower displacement are shown in Figs. 36 through 41 respectively. We can see that even for highly turbulent wind, all key turbine variables behave excellently.

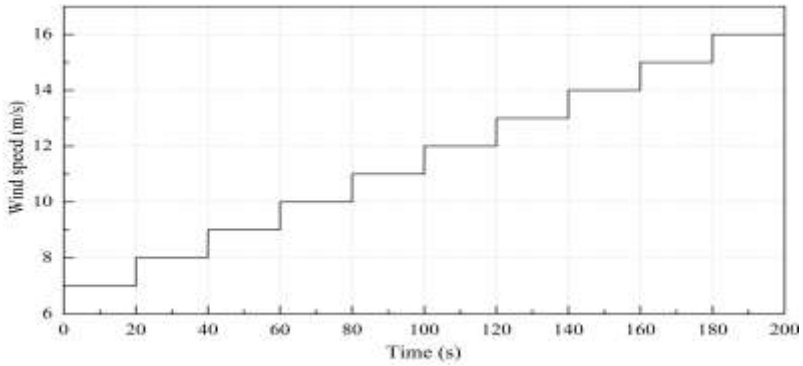

Fig. 21 Wind speed profile

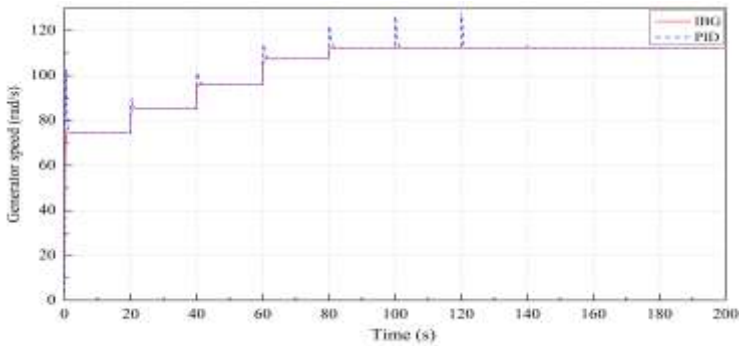

Fig. 22 Generator speed

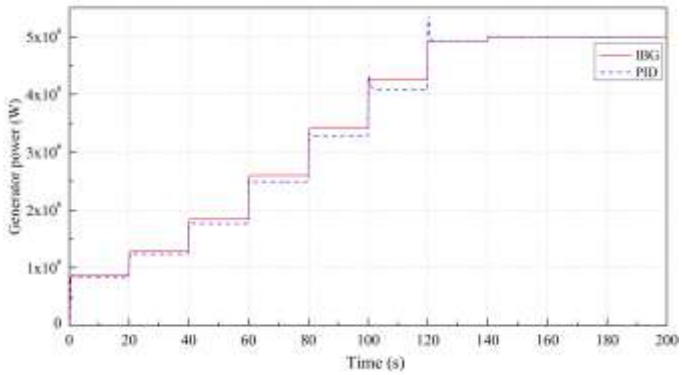

Fig. 23 Generator power

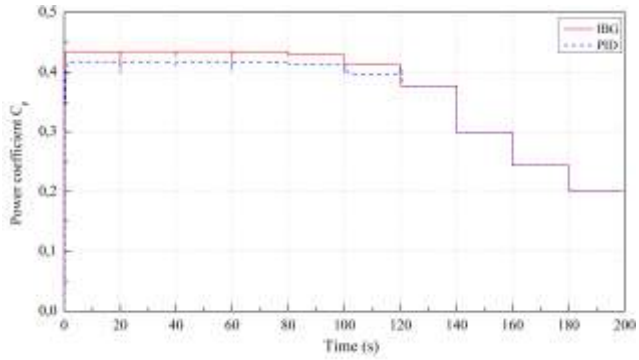

Fig. 24 Power coefficient

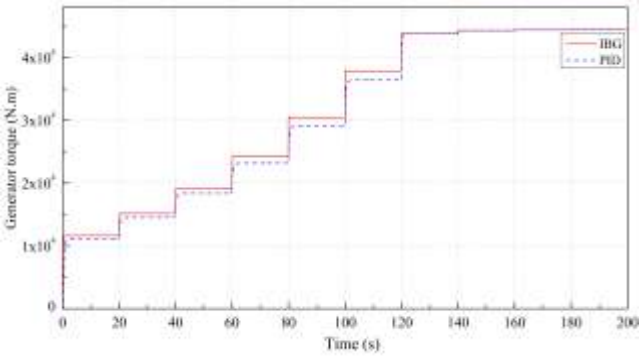

Fig. 25 Generator torque

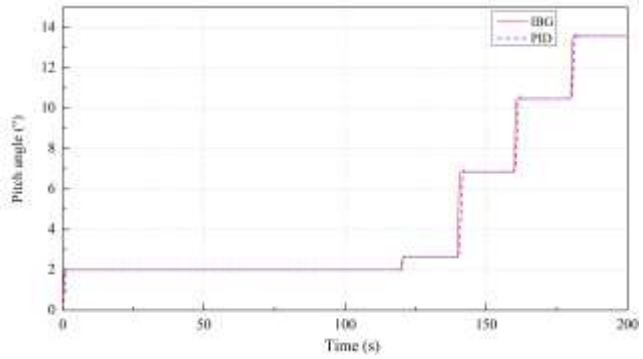

Fig. 26 Pitch angle

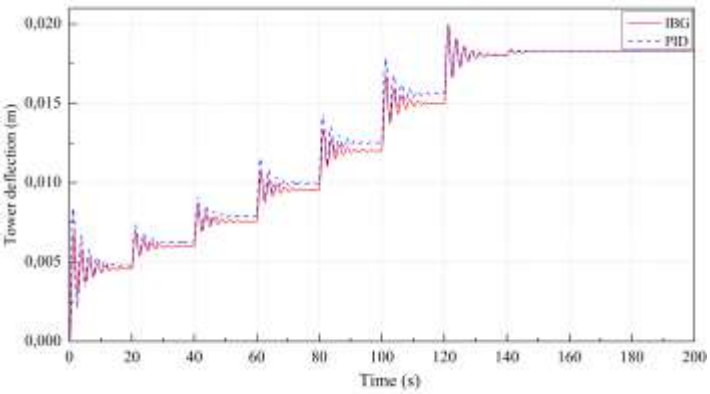

Fig. 27 Tower displacement

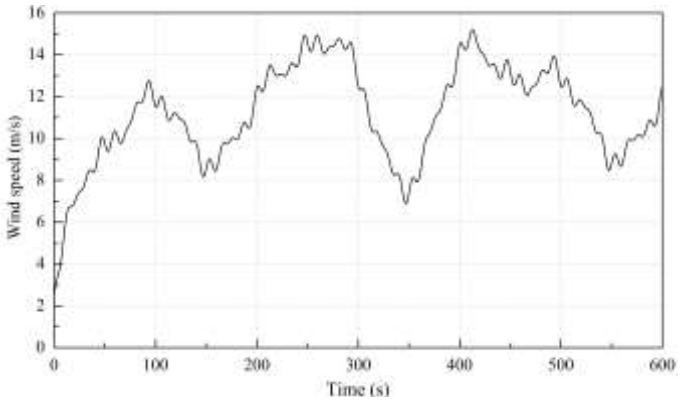

Fig. 28 Wind speed profile (12m/s)

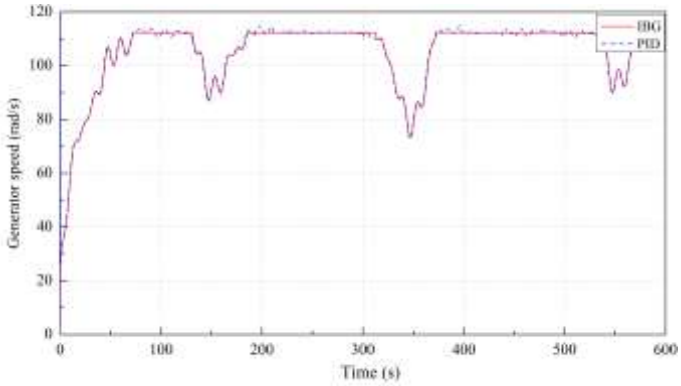

Fig. 29 Generator speed (12m/s)

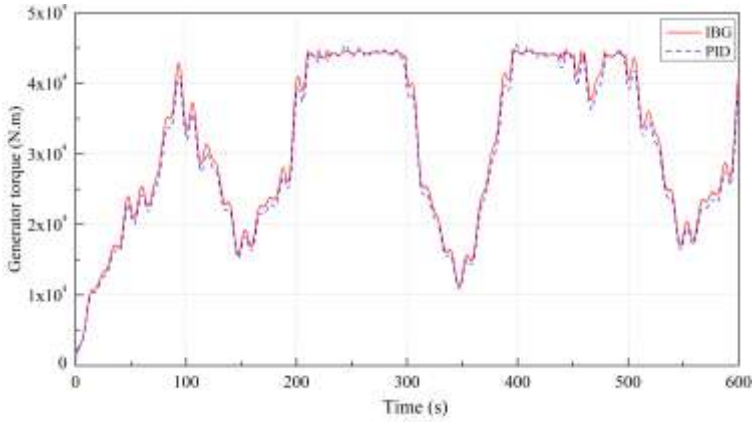

Fig. 30 Generator torque (12m/s)

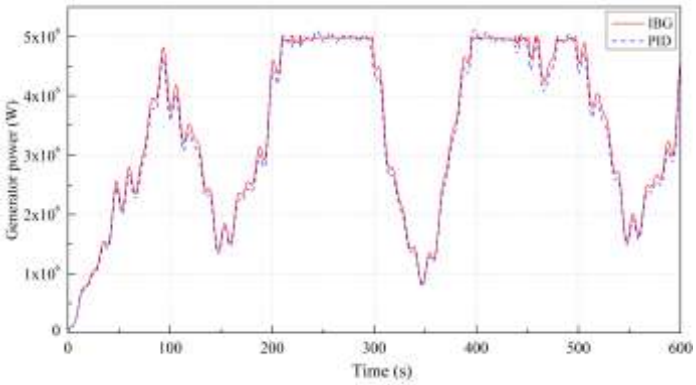

Fig. 31 Generator power (12m/s)

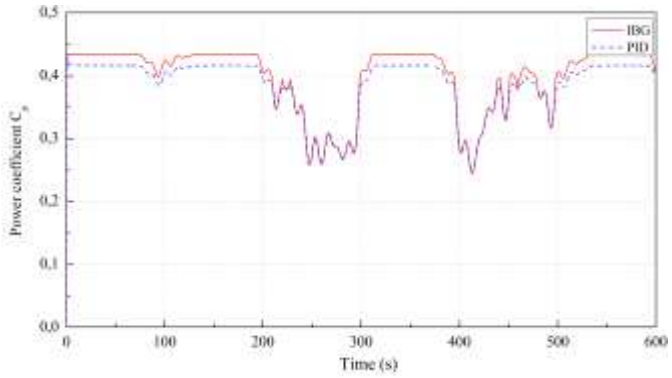

Fig. 32 Power coefficient (12m/s)

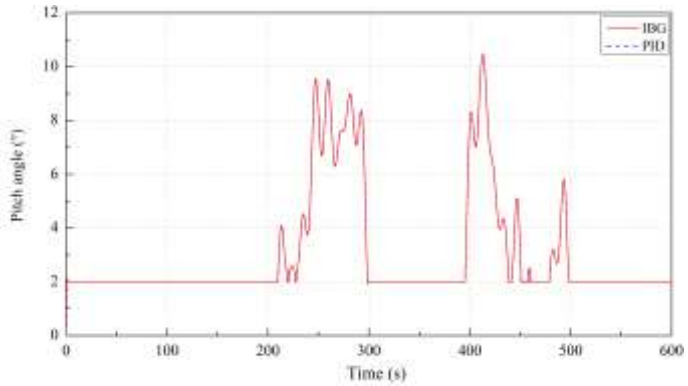

Fig. 33 Pitch angle (12m/s)

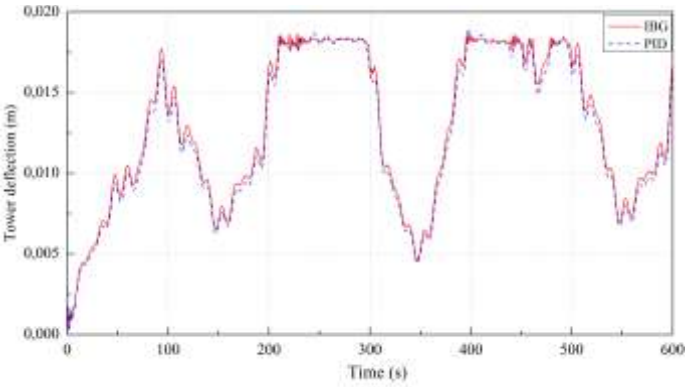

Fig. 34 Tower displacement (12m/s)

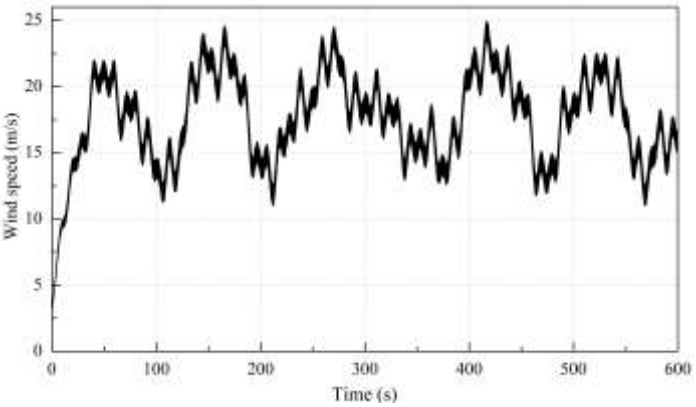

Fig. 35 Wind speed profile (18 m/s)

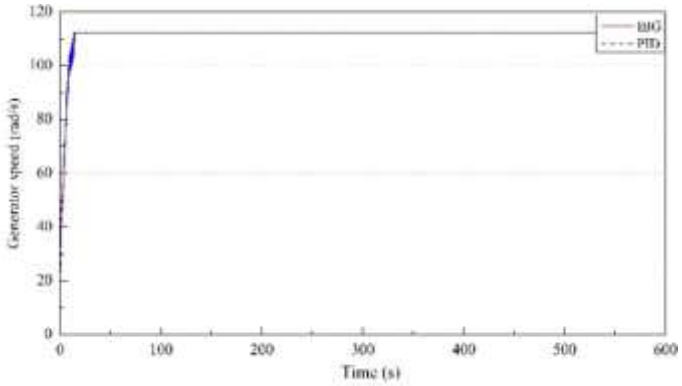

Fig. 36 Generator speed (18 m/s)

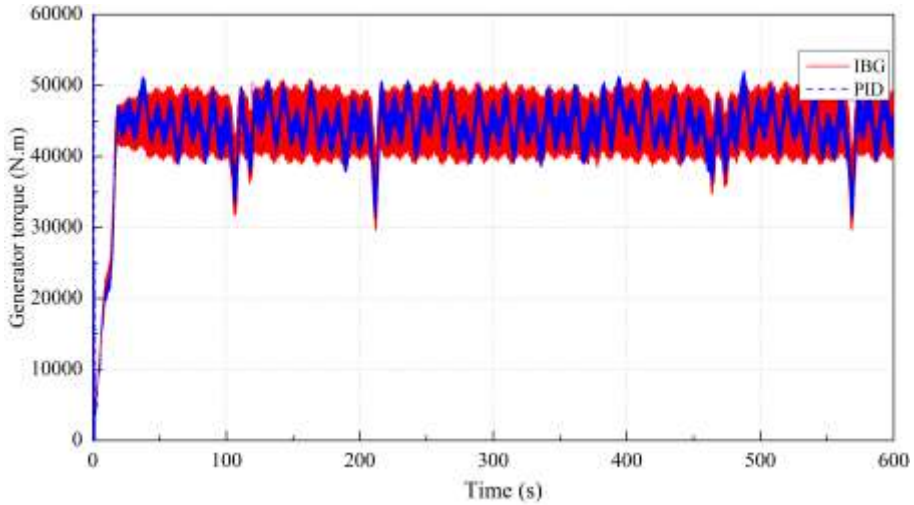

Fig. 37 Generator torque (18 m/s)

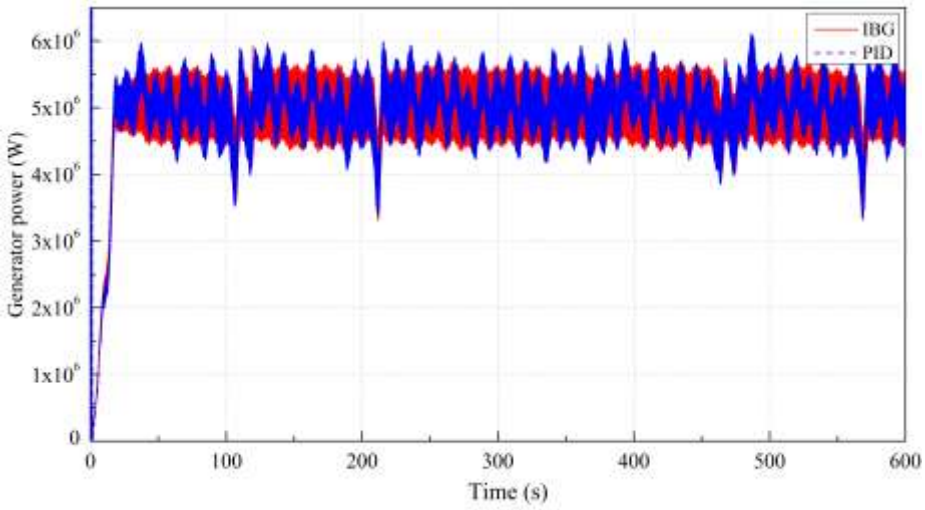

Fig. 38 Generator power (18 m/s)

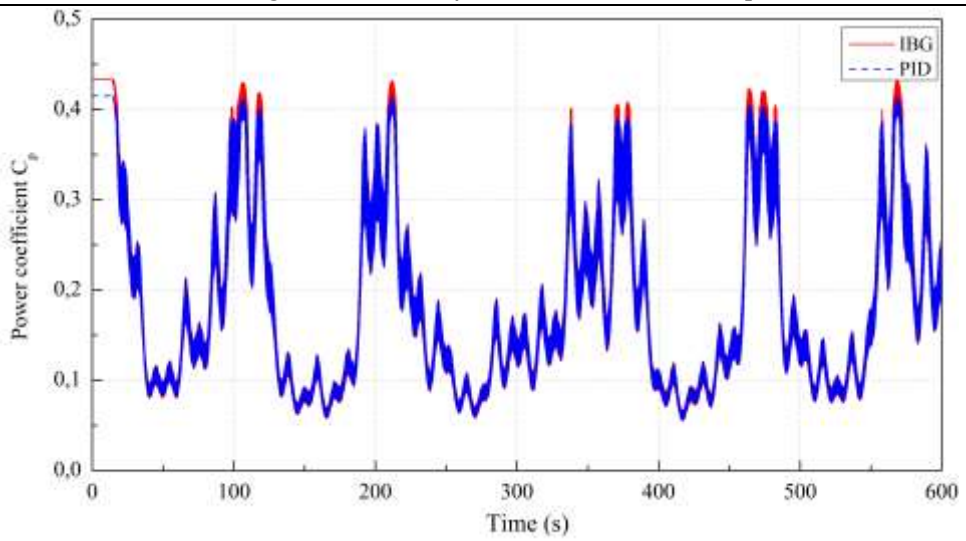

Fig. 39 Power coefficient (18 m/s)

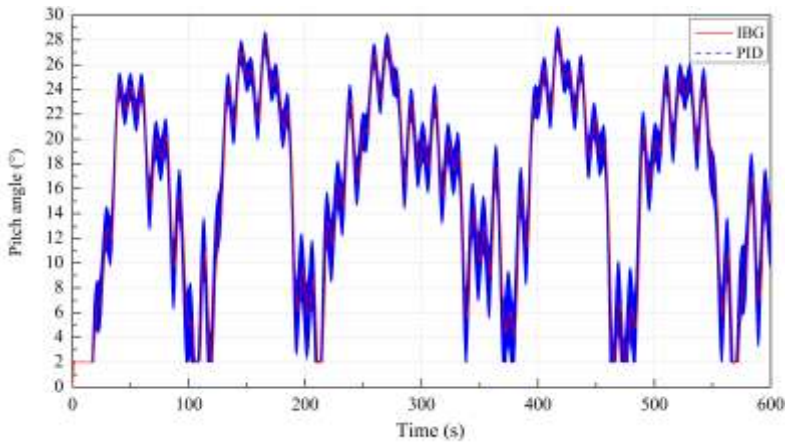

Fig. 40 Pitch angle (18 m/s)

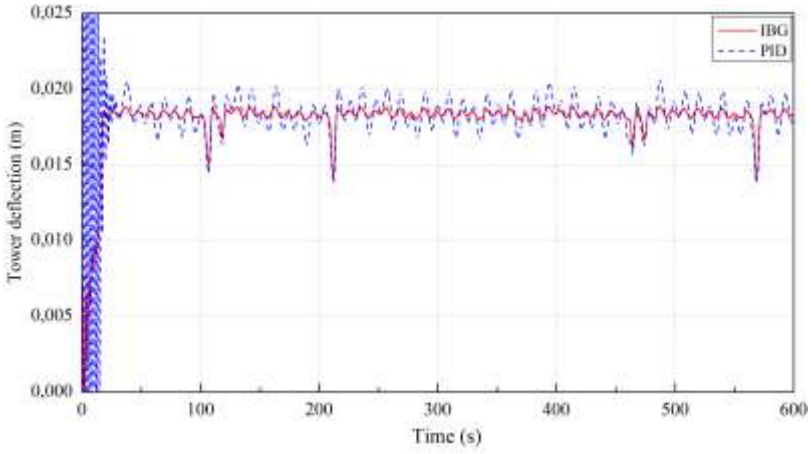

Fig. 41 Tower displacement (18 m/s)

From the three simulations, it can be concluded that, for arbitrary turbulent wind profile, the proposed control can cope well with wind variation; all key variables can meet the requirements of the wind turbine system. At the end of this simulation, we find that compared with conventional PID strategies, IBG can provide more effective performance in the wind turbine power production. Controllers designed in this paper were tested by using the 20-sim program.

VII. Conclusion and Future Work

In this paper, a mechatronic model of a wind turbine generating system using the bond graph approach is proposed to analyze and control power and speed of a variable speed variable pitch wind turbine. The proposed controllers used the bond graph model of a wind turbine in order to formulate the inverse bond graph model control. The control laws were intuitively obtained by considering this model. The paper proposed an effective control strategy which is considered for a 5MW wind turbine, including both generator torque and pitch angle control at different regions of operation of the wind turbine, including maximum power region (region II) and rated power region (region III). The control strategy was designed for a wide range of wind conditions. The main aim is to capture the maximum power in region II and regulated power and generator speed at its rated values in region III, with reduced oscillation on the tower at below rated speed. A comparison with PID controller is done. From the simulation the IBG controller can achieve the maximum and quality power in all the regions of wind speed. The simulation results show that the proposed controller has more performance that is favorable in all the regions of wind speed than the conventional PID controller; all turbine variables including pitch angle, turbine rotor speed, and power output behave excellently.

It is suggested in future research work to test the proposed control law by considering a detailed model of the induction machine using the bond graph approach, and the control law will be synthetized from the inverse bond graph model by considering the induction generator in its natural reference frame.

Appendix A: Wind turbine parameters

Parameters	Values
Rated turbine power	Pn=5MW
Rotor radius	R=55m
Air density	ρ=1.225 kg/m3
Cut-in wind speed	vcut-in=3m/s
Cut-out wind speed	vcut-out=25m/s
Rated wind speed	vrated=12m/s
Rated generator speed	ωrated=112rad/s
Rated generator torque	Trated=43KNm
Drive train	
Rotor inertia	Jr=5.9145.105Kg.m2
Rotor bearing	Dr=1000N.m.s/rad
Main speed shaft stiffness	Kms=8.7354.108N.m/rad
Main speed shaft damping	Dms=6.3478.105N.m.s/rad
Gearbox ratio	N=60:1
High speed shaft stiffness	Khs=108N.m/rad
High speed shaft damping	Dhs=1.33.103N.m.s/rad
Generator inertia	Jg=18.7kg.m2
Generator friction coefficient	Dg=0.1N.m.s/rad
Pitch system	
motor Resistance	R=3.9Ω
motor inductance	L=4.10-3H
emf constant	k=0.4
Rotor inertia of the motor	Jind=10-3Kg.m2
Rotor bearing of the motor	find=0.01N.m.s/rad
gearbox ratio	N=0.016
blade inertia	Jblade=800Kg.m2
blade dampind	Dblade=2.3.105N.m.s/rad
blade stiffness	Kblade=1.7.107N.m/rad

References

[1] Fernando D. Bianchi, Hernán De Battista and Ricardo J. Mantz. 2007. Wind Turbine Control S ystems: Principles, Modelling and Gain Scheduling Design.

[2] Burton T, Sharpe D, Jenkins N, Bossanyi E. 2001. Wind energy handbook. New York: Wiley Publications.

[3] YaxingRen, LiuyingLi, JosephBrindley, LinJiang. 2016. Nonlinear PI control for variable pitch wind turbine. Control Engineering Practice, 50: 84–94.

[4] Richie Gao, ZhiweiGao. 2016. Pitch control for wind turbine systems using optimization, estimation, and compensation, Renewable Energy, 91: 501-15.

[5] Qiao W., Zhou W.,Aller J. M., and Harley R. G. 2008. Wind speed estimation based sensorless control for a wind turbine driving a DFIG, IEEE Trans. Power Electron, 23(3): 1156–59.

[6] Yilmaz A. S. and Ozer Z. 2009. Pitch angle control in wind turbine above the rated wind speed by multilayer perception and radial basis function neural networks, IEEE Exp. Syst, 36(6): 9767–75.

[7] Liao M., Dong L., Jin L.,and Wang S. 2009. Study on rotational speed feedback torque control for wind turbine generator system, in Proceedings of the International Conference on Energy and Environment Technology (ICEET ’09), 853–56.

[8] Sheikhan M., Shahnazi R., and NooshadYousefi A. 2013. An optimal fuzzy PI controller to capture the maximum power for variablespeed wind turbines, Neural Computing and Applications, 23(5): 1359–68.

[9] Boukhezzar B., Lupu L., Siguerdidjane H., and Hand M. 2007. Multivariable control strategy for variable speed, variable pitch wind turbines, Renewable Energy, 32(8): 1273–87.
[10] Jafarnejadsani H., Pieper J., and Ehlers J. 2013. Adaptive control of a variable-speed variable-pitch wind turbine using radial-basis function neural network, IEEE Transactions on Control Systems Technolog y, 21(6): 2264–72.
[11] Zhang W.and Xu H. 2011.Active disturbance rejection based pitch control of variable speed wind turbine, in Procee dings of the 30th Chinese Control Conference, 5094–98.
[12] Jonkman J, Butterfield S, Musial W, Scott G. 2009. Definition of a 5-MW reference wind turbine for offshore system development. Technical report. Golden, Colorado. USA: National Renewable Energy Laboratory (NREL)
[13] Margolis D. 2011. Bond Graph Modelling of Engineering Systems: Theory, Applications and Software Support.
[14] Merzouki R., Samantaray A.K.,Pathak P.M. and Bouamama B.O. 2013. Intelligent Mechatronic Systems: Modeling, Control and Diagnosis.
[15] Paynter H.M. 1961. Analysis and Design of Engineering Systems (M.I.T. Press, Cambridge). rm optimization algorithm. ISA Transactions, 51: 641–48.
[16] Karnopp D.C., Margolis D.L., Rosenberg R.C. 2000. System Dynamics: Modeling and Simulation of Mechatronic Systems (Wiley, New York).
[17] Bakka T., Reza K.H. 2013. Bond graph modeling and simulation of wind turbine systems, J MechSciTechnol; 27(6): 1843–52.
[18] Heier, S. 1998. Grid Integration of Wind Energy Conversion Systems. Wiley, New York.
[19] Khaouch Z. et al. Mechatronic modeling of a 750kW fixed-speed wind energy conversion system using the Bond Graph Approach .ISA Transactions (2016) http://dx.doi.org/10.1016/j.isatra.2016.07.009i
[20] PoultagonI., Shahnazi R., Sheikhan M. 2012. RBF neural network based PI pitch controller for a class of 5-MW wind turbines using particle swarm optimization algorithm. ISA Transactions 51 (2012) 641–648.
[21] Villanueva I., Ponce P., Monina A. 2015. Interval Type 2 Fuzzy Logic Controller for Rotor Voltage of a Doubly-Fed Induction Generator and Pitch Angle of Wind Turbine Blades. IFAC-PapersOnLine, 48(3): 2195–202.
[22] Gawthrop P.J. 1995.Bicausal bond graph, in: Proceeding of the International Conference on Bond Graph Modeling and Simulation ICBGM'95, vol. 27.
[23] Gawthrop P.J. 2000. Physical interpretation of inverse dynamics using bicausal bond graphs. J. Frankl. Inst., 337(6): 743–69.
[24] Ngwompo R.F., Scavarda S. 1999.Dimensioning problems in system design using bicausal bond graphs. Simul. Pract. Theory7, 577–587.
[25] Ngwompo R.F., Scavarda S., Thomasset D. 2001. Physical model-based inversion in control systems design using bond graph representation—part 2: applications. Proc. IMechE Part I J. Syst. Control Eng, 215: 105–12.
[26] Zigeler J.G., Nichols N.B. 1942 Optimization Setting for Automatic Controller, Trans. ASME, Vol. 64, pp. 756-769.